journal

J. Am. Ceram. Soc., 84 [8] 1755–62 (2001)

Ferroelastic and Plastic Deformation of t'-Zirconia Single Crystals

Dietmar Baither,[†,‡] Martin Bartsch,[†] Bernd Baufeld,[†,§] Aleksander Tikhonovsky,[†] Andreas Foitzik,[¶,††] Manfred Rühle,[*,¶] and Ulrich Messerschmidt[†,‡‡]

Max-Planck-Institut für Mikrostrukturphysik, D-06120 Halle (Saale), Germany, and Max-Planck-Institut für Metallforschung, D-70174 Stuttgart, Germany

Polydomain tetragonal (t') zirconia was deformed in compression along a ⟨100⟩ orientation at various temperatures between 500° and 1400°C. The stress–strain curves showed a plateau corresponding to ferroelastic deformation, followed by plastic deformation at a higher yield stress level. In both ranges, the strain-rate sensitivity of the stress was measured by stress-relaxation tests. The microstructure of the tetragonal domains after ferroelastic deformation and the dislocation substructure were studied by transmission electron microscopy in a high-voltage electron microscope. As expected, ferroelastic deformation suppressed the tetragonal variant with its c-axis parallel to the loading direction. The dislocation structure consisted of intersecting dislocations on different slip systems with strongly bowed-out segments. The microprocesses of deformation are discussed here by comparing the deformation data with those of cubic zirconia deformed in the same orientation and based on the observed microstructure. The particular microstructure of t' zirconia seems to prevent recovery, so that the high flow stress of ~700 MPa is preserved up to 1400°C.

I. Introduction

Materials containing tetragonal zirconia are promising for structural applications, because of their stress-assisted tetragonal-to-monoclinic transformation near room temperature, which enables the design of zirconia-toughened ceramics, and also because of their potential for ferroelastic domain switching at high temperatures. Ferroelastic domain switching was first observed in so-called polydomain tetragonal zirconia, or t' zirconia.[1] The role of t' zirconia in toughening ceramics is reviewed elsewhere.[2] This zirconia is a metastable tetragonal phase of low stabilizer content, obtained by a diffusionless displacive transformation during quenching from the cubic phase field;[3] it consists of tetragonal domains or twin variants, which are arranged in a complicated domain and colony structure, described in more detail in Section III of this paper. The ferroelastic deformation consists of the reorientation of the tetragonal domains in the field of the applied stress. Some details of this process have been studied in numerous papers.[1,4–10] Recently, ferroelastic domain switching has been observed directly by *in situ* straining experiments inside a high-voltage electron microscope (HVEM).[11] In the course of the ferroelastic tensile deformation, only one of the three variants survived, forming a tetragonal single crystal. This crystal contained residual defects. In compression, two of the three variants may remain.

Ferroelastic domain switching in zirconia is not restricted to the t' phase. *In situ* straining experiments in the HVEM[12] and, later, X-ray diffractometry[13,14] have shown that it may also occur in the tetragonal precipitates in partially stabilized zirconia. Domain switching can have a remarkable effect on the plastic deformation or via dislocation motion. The model of precipitation hardening in partially stabilized zirconia[15] is based on the friction caused by the formation of antiphase boundary-like defects, which the dislocations have to produce in at least one of the variants composing the colonies. Ferroelastic deformation preceding plastic deformation changes the domain structure of the precipitates and, therefore, influences the motion of dislocations in the tetragonal regions of the specimen.[16]

Despite numerous studies on the ferroelastic deformation of zirconia, knowledge of the temperature and strain-rate dependence of the coercive stress, as well as of the plastic flow stress of tetragonal zirconia, is still insufficient. The present paper aims to fill this gap for compression experiments on t' zirconia, to compare the data with that on the plastic deformation of cubic zirconia, and to yield some information on the domain and dislocation structures formed by ferroelastic and plastic deformation.

II. Experimental Procedure

Specimens of ZrO_2–3 mol% Y_2O_3 measuring ~2 mm × 2 mm × 8 mm were cut along faces perpendicular to the $\langle 100 \rangle_c$ axes by a wire saw for uniaxial compression experiments. The indexing characterized by the subscript "c" relates to a pseudocubic system fixed with the specimen. The t' phase was obtained by annealing the specimens in air at 2150°C in the cubic phase field for 10 min, in a standard furnace containing a zirconia tube that had been resistance-heated to reach the high temperature. Afterward, the specimens were quenched, inside the furnace, to 1400°C within 3 min, by switching off the heating current of the zirconia tube, and then furnace-cooled to room temperature within 60 min, to prevent additional crack nucleation. Below 1400°C, diffusion is slow enough to not destroy the metastable t' structure. The whole crystal volume, in contrast to that of partially stabilized zirconia, should consist of t' phase containing a uniform concentration of the yttria stabilizer. Because the starting material was inhomogeneous and had many internal cracks, specimens of a suitable quality were difficult to prepare. Therefore, the number of experiments was quite restricted.

The compression specimens were next ground and carefully polished. Deformation tests were performed along the long $[010]_c$ axis, in a single-screw testing machine, in air, at a strain rate of $6.6 \times 10^{-6}\ s^{-1}$. Stress-relaxation tests were conducted to determine the strain-rate sensitivity of the stress, $r = d\sigma/d \ln \dot{\varepsilon}$, where σ is the stress and $\dot{\varepsilon}$ the ferroelastic or plastic strain rate. The stress-relaxation curves were plotted as stress, σ, versus the

H. Chan—contributing editor

Manuscript No. 188347. Received August 7, 2000; approved February 21, 2001. Supported by the Deutsche Forschungsgemeinschaft (DFG).

*Member, American Ceramic Society.
†Max-Planck-Institut für Mikrostrukturphysik.
‡Present address: Institut für Metallforschung, Universität Münster, D-48149 Münster, Germany.
§Present address: DLR—German Acro Space Center, Institute of Material Research, Linder Höhe, D-51147 Köln, Germany.
¶Max-Planck-Institut für Metallforschung.
††Present address: Fachbereich Mechatronik, Fachhochschule Esslingen, D-73037 Goeppingen, Germany.
‡‡Author to whom correspondence should be addressed: Max-Planck-Institut für Mikrostrukturphysik, Weinberg 2, D-06120 Halle (Saale), Germany.

logarithm of the negative relaxation rate, $\dot{\sigma}$. Because $\dot{\varepsilon}$ is proportional to $-\dot{\sigma}$ during a stress-relaxation test, the strain-rate sensitivity is given as the inverse slope of this plot:

$$r = \frac{d\sigma}{d \ln(-\dot{\sigma})} \quad (1)$$

The values of r, given in Section IV of this paper, were measured at the beginning of the relaxation tests. Thus, they correspond to the strain rate before relaxation.

One specimen, deformed at 1150°C up to a total nonelastic strain of ~0.5%, was cut into smaller pieces. One piece, measuring 0.7 mm × 1.4 mm × 1.7 mm, was deformed in the $[001]_c$ direction to show the reorientation of the tetragonal domains after an initial orientation, under load, in the $[010]_c$ direction.

Specimens for transmission electron microscopy investigations were prepared by cutting slices with a $(100)_c$ plane from the deformed specimens. These slices were ground to a thickness of ~0.1 mm, dimpled, and ion-milled down to electron microscopic transparency. These specimens were studied in an HVEM at an acceleration voltage of 1000 kV.

III. Domain and Colony Structure

Structurally, t' zirconia consists of three types of tetragonal domains or variants, denoted t_1, t_2, and t_3, depending on whether their c-axes are parallel to the x-, y-, or z-axis of the pseudocubic lattice. Two variants each are stacked along $\{101\}_t$ planes to form larger colonies, with true twin relations between the individual domains. Indexes labeled by the subscript "t" are given in a tetragonal notation, with the c components given by the third index. In the ideal case, these colonies are arranged in helical structures, to fill the whole crystal volume at minimum elastic strain energy.[17] In this way, $\{101\}_t$ twin planes constitute the interfaces between the domains inside a colony and also between domains of different colonies. Figures 1(a)–(d) show the four possible cuts through the spatial structure in the projection on the $(100)_c$ image plane of the electron micrographs. The orientations of the tetragonal axes t_2 and t_3 in the image plane are marked by the directions of the vertical or horizontal hatching. The axis t_1 out of the image plane is labeled by dots. In Figs. 1(a) and (b), the domain boundaries are inclined by 45° with respect to the image plane. The colony boundaries are $(01\bar{1})_c$ planes in Fig. 1(a) and $(011)_c$ planes in Fig. 1(b), oriented edge on. The t_1 variant extends through both types of colonies in both figures. In Fig. 1(c), the domain boundaries are edge on in the upper and lower parts but inclined in the central part. The colony boundaries emerging through the surface in the horizontal direction are inclined with respect to the image plane. The variant t_3, with horizontal hatching, extends through all colonies. Figure 1(d) can be understood analogously.

Figure 2 shows electron micrographs of the respective structures. Figure 2(a) corresponds to Fig. 1(a) and Fig. 2(b) to Fig. 1(d). The electron microscopy contrasts inside the domains in Fig. 2(a) are (probably) caused by antiphase domain boundaries. The degree of perfection of the domain and colony structure seems to depend on the rate of quenching from the cubic phase field. The relatively perfect structures of Fig. 2 are obtained by quenching to 1400°C in 3 min, as described in Section II of this paper. More rapid quenching results in less perfect structures, as demonstrated in Fig. 3.

IV. Results of Macroscopic Deformation Tests

Figure 4 shows a stress–strain curve of the ferroelastic and plastic deformation of t' zirconia at 500°C. After elastic loading, ferroelastic deformation usually starts at a well-defined coercive, or transformation, stress, σ_t. At 500°C, the stress does not increase during ferroelastic deformation. At higher temperatures, the specimens harden during ferroelastic deformation, with total hardening coefficients of ~25 GPa at 1000°C and ~33 GPa at 1400°C. After the ferroelastic deformation is exhausted, the stress increases again. The ferroelastic transformation strain, $\Delta\varepsilon_t$, measured up to the inflection point of the second elastic range, varies between 0.3% and 0.47%. Plastic deformation is characterized by the yield stress, σ_y. At 500°C, the deformation curve exhibits a well-defined yield drop that is missing at higher temperatures. Deformation in the present experiments was stopped at relatively low plastic strains, to avoid fracture. Thus, the plastic work-hardening behavior was not studied.

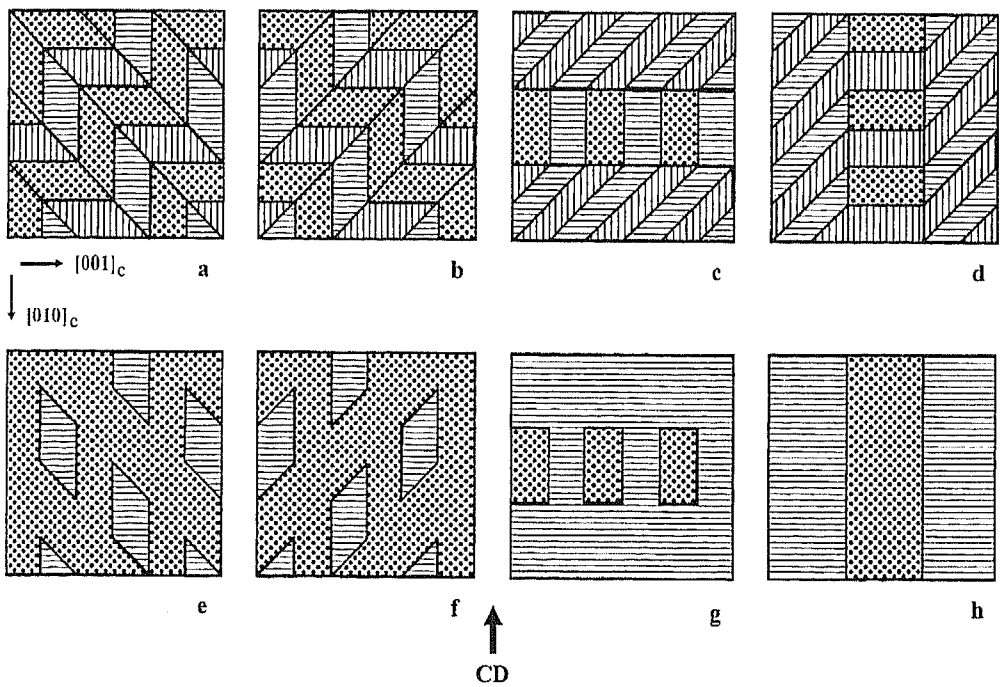

Fig. 1. (a)–(d) Four possible cuts through the domain and colony structure of t' zirconia, along the $(100)_c$ image plane of the electron micrographs (directions of the c axes are marked by hatching; ratio of domain thickness to width is increased with respect to the micrographs). (e)–(h) Respective structures after ferroelastic domain switching, in compression, along the $[010]_c$ axis ("CD" denotes the compression direction).

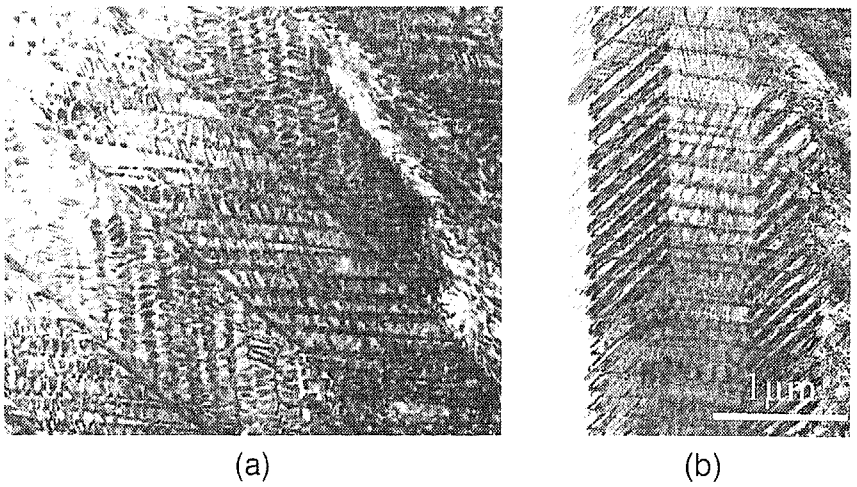

Fig. 2. Electron micrographs of domain and colony structures: (a) domain boundaries inclined with respect to the image plane and colony boundaries edge on, as in Fig. 1(a), and (b) colony boundaries inclined as in Fig. 1(d).

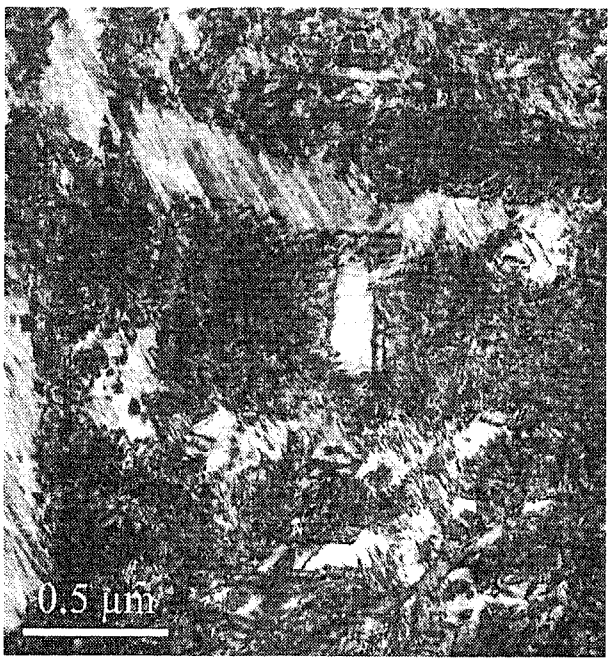

Fig. 3. Domain and colony structure of lower perfection, as a result of a higher quenching rate from 2150° to 1400°C.

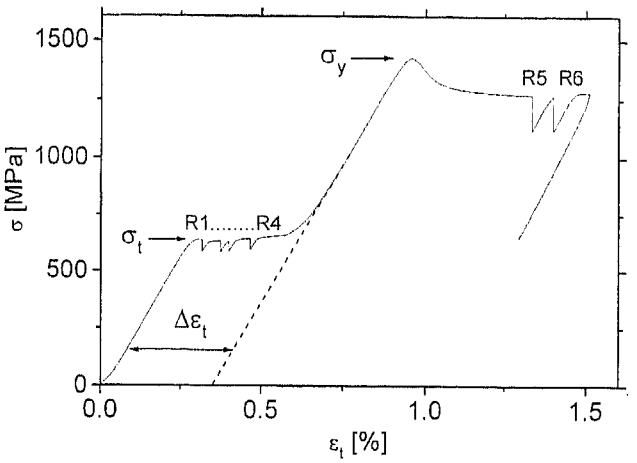

Fig. 4. Stress–strain curve of ferroelastic and plastic deformation of t' zirconia at 500°C (ε_t is total strain, $\Delta\varepsilon_t$ transformation strain, σ_t coercive stress, σ_y plastic yield stress, and R1–R6 stress-relaxation tests).

Figure 5 presents the temperature dependence of σ_t and σ_y. Both values decrease with increasing temperature, σ_t very moderately. Figure 5 also shows the flow stresses of cubic zirconia with 10 mol% yttria in the soft ⟨112⟩ orientation and the ⟨100⟩ orientation, corresponding to the present experiments on t' zirconia. At the lowest temperatures, σ_t is on the order of the flow stress of cubic zirconia in the ⟨112⟩ direction. Up to ~1000°C, σ_t is clearly lower than the flow stress of cubic material in the same ⟨100⟩ loading direction, but at 1400°C, σ_t is higher. At the lowest temperature, the σ_y value of t' zirconia equals that of cubic zirconia, but at high temperatures the value is much higher.

To study the strain-rate sensitivity, r, of the stress, stress-relaxation tests were performed during both the ferroelastic and the plastic deformation, as indicated by R1–R6 in Fig. 4. Some typical stress-relaxation curves are presented in Fig. 6. At 500°C, the plot of ln $(-\dot{\sigma})$ vs σ of ferroelastic deformation shows a slight "normal" bending toward the stress axis. At 1400°C, the relaxation curve shows two clear stages, a very steep decrease at the beginning and a very flat component at longer relaxation times. The relaxation curves of plastic deformation always exhibit "normal" curvature. As described in Section II of this paper, r is represented by the inverse slope of the relaxation curves. Data taken at the beginning of the curves are plotted in Fig. 7 as a function of temperature. Generally, the strain-rate sensitivity of ferroelastic deformation is lower than that of plastic deformation, and the value decreases continuously as temperature increases. At 1400°C, only the low value is plotted, corresponding to the very steep component at the beginning of the relaxation curves. The flat component of the relaxation curve yields r values between 20 and >100 MPa. The r values of plastic deformation of t' zirconia between 500° and 600°C fall from a high value down to 15–20 MPa. Too few measurements are available to allow a decision on whether the values remain constant at higher temperatures or show a minimum between 900° and 1000°C, as do those of cubic zirconia in the same orientation. However, the values for cubic zirconia increase to much higher values at high temperatures.

As described earlier, in Section II, part of the specimen that had been deformed at 1150°C along $[010]_c$ was later deformed, at the same temperature, along $[001]_c$, to observe the reorientation of the tetragonal domains. Figure 8 presents the stress–strain curve. The coercive stress of ~150 MPa is only about one-third that of the initial deformation, while the plastic yield stress of ~820 MPa is slightly higher than the original value. The strain-rate sensitivities of ferroelastic deformation, 2.3 MPa, and of plastic deformation, ~22 MPa, approximately equal those of the initial deformation.

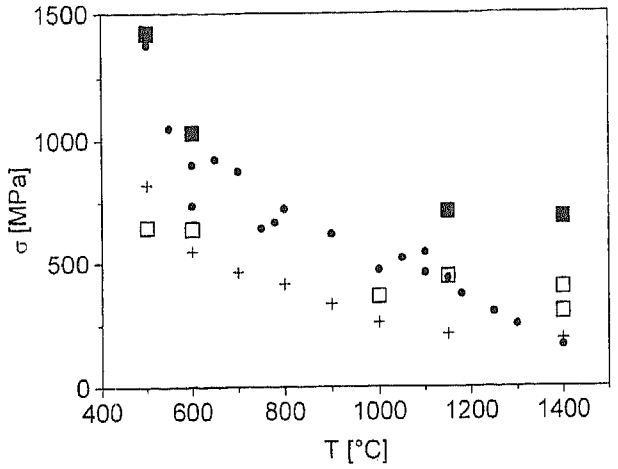

Fig. 5. Temperature dependence of (□) σ_t and (■) σ_c of t' zirconia along $\langle 100 \rangle_c$, at a strain rate of 6.6×10^{-6} s^{-1}, compared with the yield stress of cubic zirconia (+) in $\langle 112 \rangle$ compression direction, at 10^{-6} s^{-1} and (●) in $\langle 100 \rangle$ direction at 10^{-5} s^{-1}.

V. Domain and Colony Structure after Ferroelastic Deformation

The specimens for electron microscopic investigations were prepared from the specimens after ferroelastic and plastic deformation at 1150°C. Thus, those specimens exhibit the domain and colony structures resulting from the ferroelastic transformation and also the dislocation structures produced during the plastic deformation. The occurrence of the three tetragonal variants after deformation can be checked by the existence of $\{112\}_t$ reflections in the diffraction patterns. Figure 9(a), of the $[1\bar{1}0]_c$ pole, shows $(11\bar{2})_c$ reflections, indicating that t_3 exists. In Fig. 9(b), of the $[10\bar{1}]_c$ pole, $(12\bar{1})_c$ reflections are missing, so that t_2, with its tetragonal axis parallel to the compression direction, does not exist. This finding is confirmed by Fig. 9(c), of the $[11\bar{1}]_c$ pole, the $(2\bar{1}1)_c$ and $(11\bar{2})_c$ reflections of which indicate that t_1 exists, in addition to t_3. Thus, ferroelastic compression along $[010]_c$ has been suppressed t_2, as expected.

Figure 10 shows an overview of the microstructure after deformation. The contrast of the individual domains disappears, but the regions of the former colonies are imaged in strong contrast. Figures 1(e)–(h) show schematically the possible structures after ferroelastic transformation, resulting from the four cuts through the microstructure in Figs. 1(a)–(d). The transformation appears in such a way that the t_2 domains always assume the character of their neighboring domains in the same colony, so that the neighboring domains become tetragonal single-crystal regions, and the high-energy pseudotwin boundaries, where a c direction in one domain has to join an a direction of another, are generated only along the narrow areas along the former colony boundaries. In the extreme case of Fig. 1(h), all colonies become uniform tetragonal grains, joining along true twin boundaries. This is the structure observed in most micrographs in a nonperfect way, as in Fig. 10. In any case, the ferroelastic deformation destroys the original domain structure and leads, at least in part of the crystal, to regions of the former colony size with a unique orientation of the c-axes t_1 and t_3.

VI. Dislocation Structure after Ferroelastic and Plastic Deformation

Figure 11 presents dislocation structures imaged with the $(022)_c$ and $(02\bar{2})_c$ reflections near the $[100]_c$ pole. Clear images of dislocations are not easy to obtain, because of the superimposed contrasts of planar defects discussed later. In each part of Fig. 11, one set of dislocations is imaged and another is extinguished. Thus, presupposing that only Burgers vectors exist parallel to the $\langle 110 \rangle_c$ directions, the Burgers vectors in Figs. 11(a) and (b) are parallel to $[011]_c$ and $[01\bar{1}]_c$ within the $(100)_c$ image plane. No other Burgers vectors parallel to $\langle 110 \rangle_c$ directions have been observed. Those parallel to $[101]_c$ and $[10\bar{1}]_c$ have zero orientation factors. Those parallel to $[110]_c$ and $[1\bar{1}0]_c$ should be extinguished at the $(002)_c$ reflection and should be visible at all other reflections at the $[100]_c$ pole, e.g., in Figs. 11(a) and (b), but that is not the case.

In the tetragonal structure, Burgers vectors of type $\frac{1}{2}\langle 110 \rangle_t$ within the basal plane are complete Burgers vectors, whereas those of $\frac{1}{2}\langle 101 \rangle_t$ in nonbasal planes lead to the production of antiphase boundary-like planar defects during the dislocation motion. Thus, the dislocations observed in this study do not produce planar defects in the t_1 variant, but they have to do so in the t_3 variant. Contrasts of planar defects are visible in Fig. 12. These antiphase boundary-like defects are responsible for the strong contrasts between the colonies in the deformed material.

Possible slip planes in zirconia are of types {100}, {110}, and {111}. The first types are excluded here because of their zero orientation factor for deformation along ⟨100⟩. The micrographs of the present study do not yield a clear decision between the latter two systems. The $\{110\}_c$ planes belonging to the observed Burgers vectors are imaged almost edge on in the micrographs taken near the $[100]_c$ pole, as in Fig. 11, whereas the respective $\{111\}_c$ planes appear under an angle of ~55°. The dislocations in Fig. 11 are aligned in the Burgers vector directions, but not very strictly. Considering that the incident beam is tilted out of the pole by only a few degrees, this finding agrees better with the assumption of $\{111\}_c$ than of $\{110\}_c$ as the activated slip planes. All dislocations show strongly bowed-out segments of lengths on the order of 0.1–0.15 μm. Figure 13 presents the microstructure imaged with a $[0\bar{2}0]_c$ reflection, where both sets of dislocations are visible. This figure demonstrates that the dislocations of the different activated slip systems pin each other by mutual intersections during multiple slip. The dislocation-density values are on the order of 2×10^{13} to 8×10^{13} m^{-2}.

VII. Microstructure after the Second Deformation

During the second deformation, along a direction perpendicular to the first, numerous small, planar defects form. The superposition of their contrasts prevents analysis of individual defects, even in very thin regions of the specimen. However, these defects cause specific additional spots in the diffraction patterns. Planar faults cause a degeneration of the reciprocal lattice points into spikes perpendicular to the fault plane and parallel to the direction of the electron beam.[18] The parallel spikes are equivalent to those arising in thin foils. If the Ewald sphere exactly cuts the reciprocal lattice points, no splitting of the spots occurs. At deviations from the reciprocal lattice points, additional spots appear. Their position with respect to the spots of the undistorted lattice is determined by the projection of the intersection points of the Ewald sphere with the spikes onto the image plane. As a characteristic feature, the position of these additional spots changes even with a slight tilting of the specimen. In the diffraction pattern of Fig. 14(a), taken near the $[100]_c$ pole, the "normal" spots expected for the undistorted lattice are not split, because their deviations from the Ewald sphere are negligible. The additional spots, at the positions of spots in a primitive cubic lattice, result from degeneration of the reciprocal lattice points of the second Laue zone into long spikes. The diffraction pattern of Fig. 14(b) was taken with the specimen tilted by ~25° toward the $[20\bar{1}]_c$ pole, around the $[020]_c$ axis. Here, the typical splitting of the spots is shown. Additional spots, which appear along the $[102]_c$ direction (perpendicular to the $[020]_c$ axis) on both sides of the normal spots, belong to the planar defects on the $(101)_c$ and $(10\bar{1})_c$ planes. The other set of additional spots deviates by ~24° from the $[020]_c$ tilting axis, symmetrical on both sides of the normal spots toward the $[102]_c$ direction. These spots are related to the defects on the $(110)_c$ and $(1\bar{1}0)_c$ planes.

Figure 15(a) is a dark-field image of the planar defects imaged by such an additional spot. Thus, the entire area of the defects

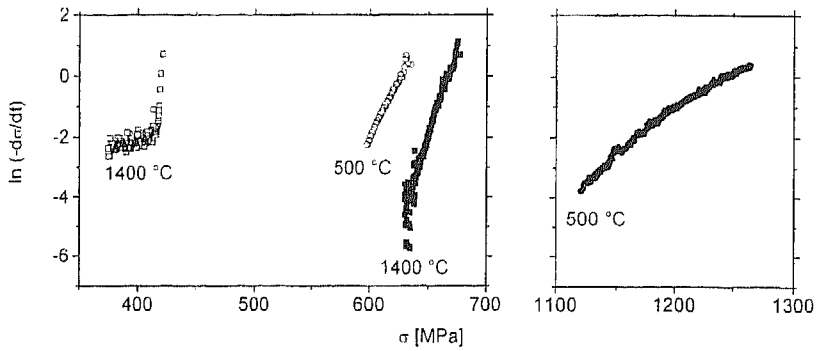

Fig. 6. Stress-relaxation curves measured during ferroelastic deformation (open symbols) and plastic deformation (filled symbols).

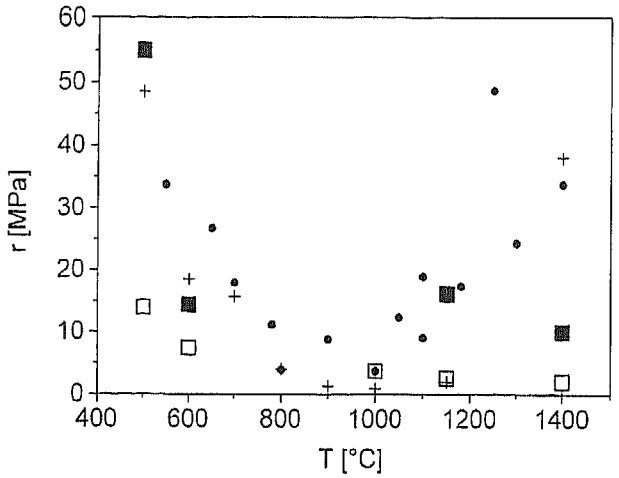

Fig. 7. Temperature dependence of the strain-rate sensitivity, r, of the stress during (□) ferroelastic and (■) plastic deformation, for t' zirconia. For comparison, data are shown for plastic deformation of cubic zirconia along the (+) ⟨112⟩ and (●) ⟨100⟩ compression axes.

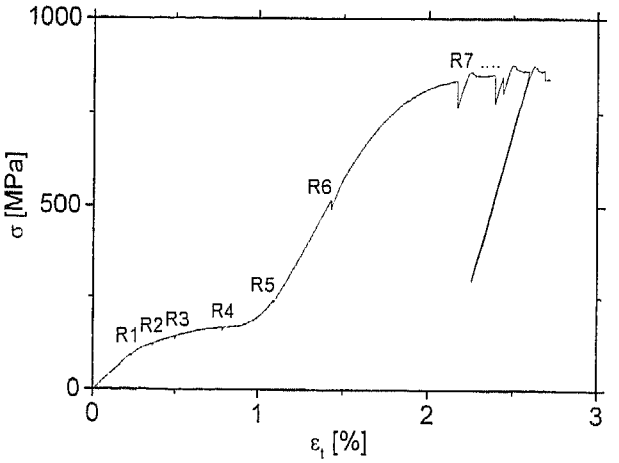

Fig. 8. Stress–strain curve taken during deformation at 1150°C, along $[001]_c$, of a specimen deformed initially at the same temperature, along $[010]_c$.

appears in bright contrast. The boundary of these defects becomes preferentially visible if a weakly excited normal spot is taken for imaging, as in Fig. 15(b).

No similar small, planar defects are detected after the first deformation. Therefore, they are assumed to have been created during the second deformation, in the interior of the large t' single-crystalline regions (t_3), which arose during the first transformation. During the second deformation, these large regions do not transform into t_1 or t_2, as a whole. Probably, the transformation starts simultaneously at many nucleation sites. If these individual domains grow, they frequently will not fit at the boundary to the adjacent one, so that antiphase domain boundaries are formed.

VIII. Discussion

(1) Ferroelastic Deformation

In t' zirconia, the c/a value amounts to ~1.01.[19] Because only one of the three variants changes the orientation of its c-axis during compression, the maximum ferroelastic strain should amount to about one-third of one percent. Such ferroelastic strains have been observed experimentally, indicating that the transformation must have been quite complete. As shown in Fig. 5, the coercive stress, σ_t, decreases by ~45% between 500° and 1400°C; i.e., it shows a weak temperature dependence. The present value at 1000°C is roughly equal to that given by Foitzik *et al.*,[10] of 285 MPa, but lower than those cited by Chan *et al.*[5] and Prettyman *et al.*,[7] of ~750 MPa. Below ~1100°C, $\sigma_t < \sigma_y$, so that ferroelastic deformation precedes plastic deformation. Only a single value, at 1000°C, of the strain-rate sensitivity of the coercive stress, $\Delta\sigma_t/\Delta \ln \dot{\varepsilon}$, can be found in the literature.[10] In Fig. 7, $\Delta\sigma_t/\Delta \ln \dot{\varepsilon}$ decreases continuously as the temperature increases. The value is remarkably lower than that of the flow stress, $\Delta\sigma_y/\Delta \ln \dot{\varepsilon}$, at the same compression direction, except at 1000°C. The low values of the strain-rate sensitivity of the coercive stress indicate that this stress has a well-defined level. However, at 1400°C, the stress-relaxation curve exhibits an almost horizontal component after the first steep decrease of the strain rate (Fig. 6). Such two-stage relaxation curves are observed during plastic deformation of cubic zirconia at the same temperature along ⟨112⟩.[20] The process causing deformation at a fixed rate under decreasing stress is not yet clear.

As shown by *in situ* straining experiments in an HVEM, tensile deformation of t' zirconia along a $\langle 100 \rangle_c$ direction results in a tetragonal single crystal, with its c-axis parallel to the tensile direction.[11] In contrast, the microstructure after compressive deformation along $[010]_c$ still contains the two tetragonal variants, t_1 and t_3, with their c-axes perpendicular to the compression direction. However, the original sequence of individual domains is destroyed, at least in part of the colonies, and changed into tetragonal single-crystal regions of the size of the former colonies.

(2) Plastic Deformation

The characteristics of plastic deformation of t' zirconia have not been described before. In cubic zirconia, three temperature ranges of the deformation can be distinguished.[21] Below ~1000°C, the deformation is controlled by thermally activated glide over obstacles and by the Peierls mechanism at the lowest temperatures. Between ~1000° and 1100°C, the deformation is of an athermal nature; above this range, recovery controls the deformation. As shown in Fig. 5, different orientations, the ⟨112⟩ orientation for easy slip on {100} planes and the present ⟨100⟩ orientation, particularly influence the low-temperature ranges where the lattice resistance is important. At 1400°C, when recovery controls the

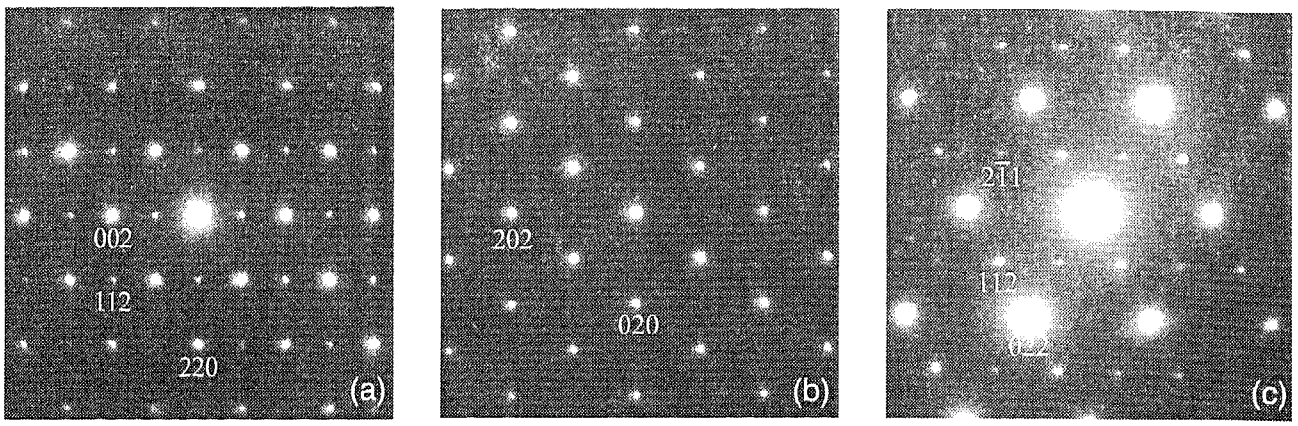

Fig. 9. Diffraction patterns of t' zirconia deformed at 1150°C, up to ~1.3%: (a) $[1\bar{1}0]_c$ pole, (b) $[10\bar{1}]_c$ pole, and (c) $[11\bar{1}]_c$ pole.

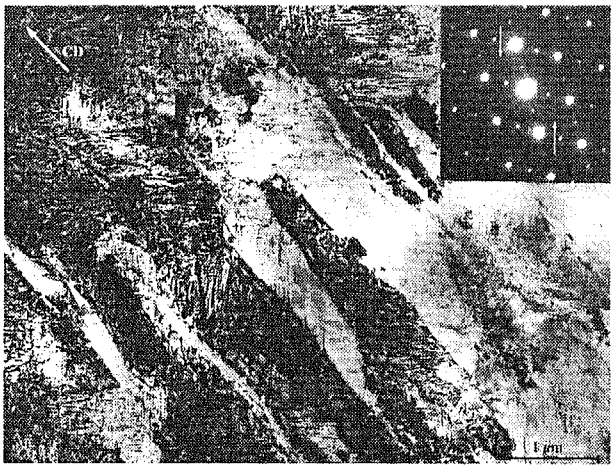

Fig. 10. Overview of the microstructure of t' zirconia after deformation at 1150°C, up to 1.3%, near the $[100]_c$ pole, $\vec{g} = (002)_c$ ("CD" denotes the $[010]_c$ compression direction). Inset: diffraction pattern at $[11\bar{1}]_c$ pole (→) missing reflections of {112} type).

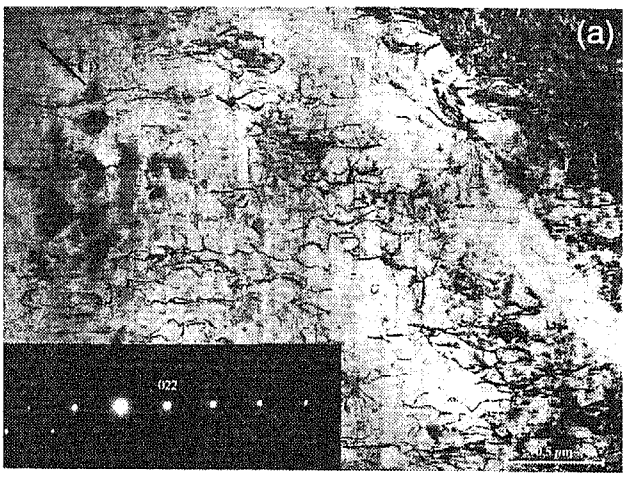

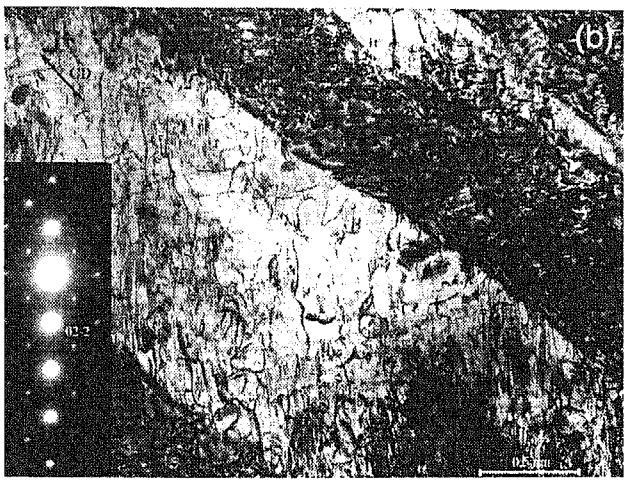

Fig. 11. Microstructure after deformation at 1150°C, up to 1.3%, near the $[100]_c$ pole: (a) $\vec{g} = (022)_c$ and (b) $\vec{g} = (02\bar{2})_c$ ("CD" denotes the compression direction).

deformation, the flow stresses along both orientations become equal. The three ranges are expressed by the strain-rate sensitivity in Fig. 7, which exhibits a strong minimum at 1000°C, corresponding to the athermal behavior. The strain-rate sensitivity is high both at low temperatures, because of the thermally activated dislocation glide, and at high temperatures, because of recovery.

The plastic flow stress, σ_y, of t' zirconia may be compared with that of cubic zirconia along the same ⟨100⟩ orientation. Previous published data on cubic zirconia are restricted to temperatures >1200°C.[22] According to Fig. 5, both flow stresses are equal at low temperatures; i.e., the different stabilizer concentrations and the microstructure formed after ferroelastic deformation do not influence the lattice resistance of dislocation glide at low temperatures. However, although the flow stress of cubic zirconia decreases drastically, down to ~200 MPa, at 1400°C, that of t' zirconia remains at the high level, ~700 MPa, up to this temperature. In accordance with this observation, the strain-rate sensitivities of both materials are similar at low temperatures, but at 1400°C, t' zirconia has a much lower strain-rate sensitivity than does cubic zirconia. In the cubic zirconia, deformation at high temperatures supposedly is controlled by recovery.[20,21,23] Thus, the main effect of the t' microstructure seems to be that it suppresses recovery. As concluded by Chen and Heuer,[24] from a dislocation-loop shrinkage study in cubic zirconia, the cation diffusion coefficient, which should control the recovery, decreases strongly as the stabilizer content increases, leading to a reduced recovery and, thus, a higher flow stress at a higher stabilizer concentration. Because the yttria concentration in t' zirconia is low, this effect cannot explain the high flow stress of this material, which certainly results from the remaining defect and domain structure.

During plastic deformation, the dislocations move in the structure produced by the ferroelastic deformation; i.e., there are at least channels of the former colony size of uniform tetragonal orientation. As mentioned already in Section VI of this paper, dislocations with Burgers vectors of the type $\frac{1}{2}\langle 110\rangle_t$ in the basal plane do not have to produce antiphase boundary-like defects. Therefore, these

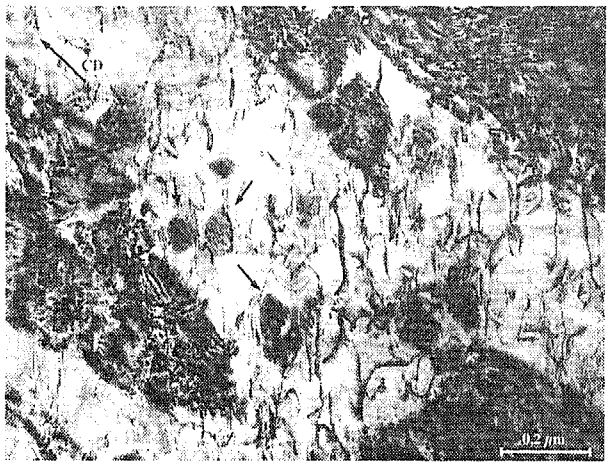

Fig. 12. Section of the microstructure showing planar defects at dislocations labeled by arrows ("CD" denotes the compression direction).

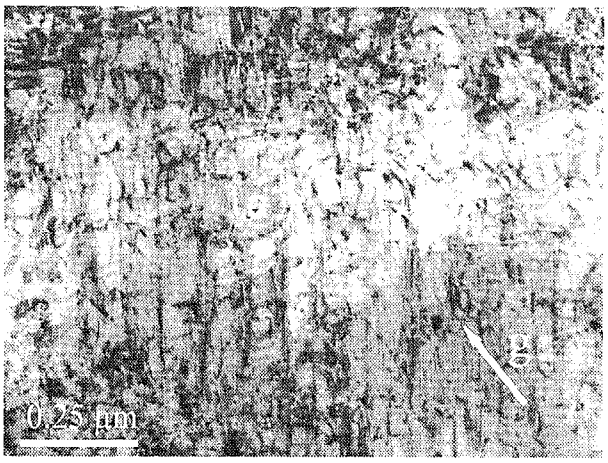

Fig. 13. Microstructure after deformation at 1150°C, near the $[100]_c$ pole, $\vec{g} = (0\bar{2}0)_c$, showing both sets of dislocations.

dislocations are not subjected to an additional glide resistance. However, when the dislocations enter the neighboring colony, they have to produce antiphase boundary-like defects, either in the whole colony, if it is of a uniform tetragonal orientation, as in Fig. 1(h), or in a set of domains, as in Fig. 1(g). Messerschmidt and co-workers[16,25] argue that the antiphase boundary-like defects on the $\{101\}_t$ planes have a low energy, which corresponds to a (shear) friction stress considerably lower than 60 MPa. Thus, the creation of these defects on $\{101\}_t$ planes contributes only weakly to the increase of the flow stress of t' zirconia with respect to that of cubic zirconia in the same orientation. Most probably, the energy of the antiphase boundary-like defects on the $\{111\}_t$ planes is also lower than the high value on the $\{100\}_t$ planes.

The contribution to the flow stress of the long-range interaction between parallel dislocations of a density ρ can be written as[21]

$$\tau_\rho = \frac{\alpha\, bKF_m\, \rho^{1/2}}{2\pi} \tag{2}$$

where α is a numerical constant equal to ~8, b the absolute value of the Burgers vector, K the energy factor of a dislocation in anisotropic elasticity, and F_m a maximum interaction constant of dislocation bypassing. The product KF_m was calculated by Messerschmidt *et al.*[21] as 53 and 35 GPa for screw and edge dislocations, respectively, on $\{111\}$ planes in cubic zirconia, yielding, with an average value of $\rho = 5 \times 10^{13}$ m^{-2}, $\tau_\rho = 175$ MPa for screw dislocations and $\tau_\rho = 116$ MPa for edge dislocations. Considering the orientation factor of 0.41, the long-range contribution to the flow stress, σ_ρ, may be on the order of 355 MPa.

Section VI of this paper showed that dislocations of different slip systems impede each other, leading to bowed-out segments with lengths, l, of 0.1–0.15 μm. In the critical configuration, these bowed-out segments produce a back stress:[21]

$$\tau_b = \frac{Kb}{2\pi l} \ln\left(\frac{l}{5b}\right) \tag{3}$$

For a screw dislocation with $K = 80.4$ GPa and $l = 0.125$ μm, the back stress amounts to $\tau_b \cong 160$ MPa or $\sigma_b \cong 390$ MPa. Consequently, the sum of the athermal components, σ_ρ and σ_b, explains well the flow stress of t' zirconia in the high-temperature range. Because the particular t' structure modified by ferroelastic deformation prevents recovery at high temperatures, these materials may be suitable components for high-temperature structural applications.

The very low coercive stress during the second deformation, with a compression direction perpendicular to the first, may indicate that the original domain boundaries are pinned—e.g., by segregation of impurities—whereas the newly created boundaries are not. Besides, the first deformation destroys the initial stable domain and colony structure of minimum elastic strain energy. The very high flow stress may result from latent hardening by the dislocations introduced during the first deformation.

IX. Conclusions

(1) Polydomain tetragonal (t') zirconia shows ferroelastic deformation. In compression, the variant with its c-axis parallel to

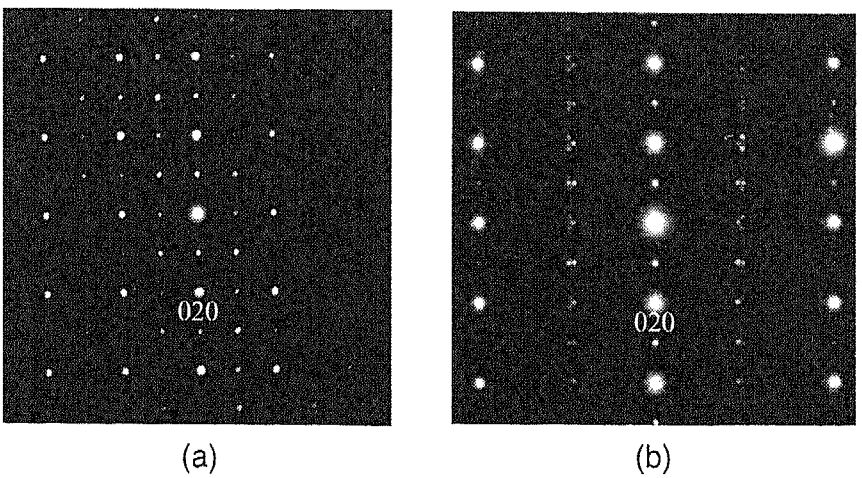

Fig. 14. Diffraction patterns after the second deformation in the $[001]_c$ direction: (a) near the $[100]_c$ pole and (b) after tilting of the specimen by ~25° toward the $[20\bar{1}]_c$ pole, around the $[020]_c$ axis.

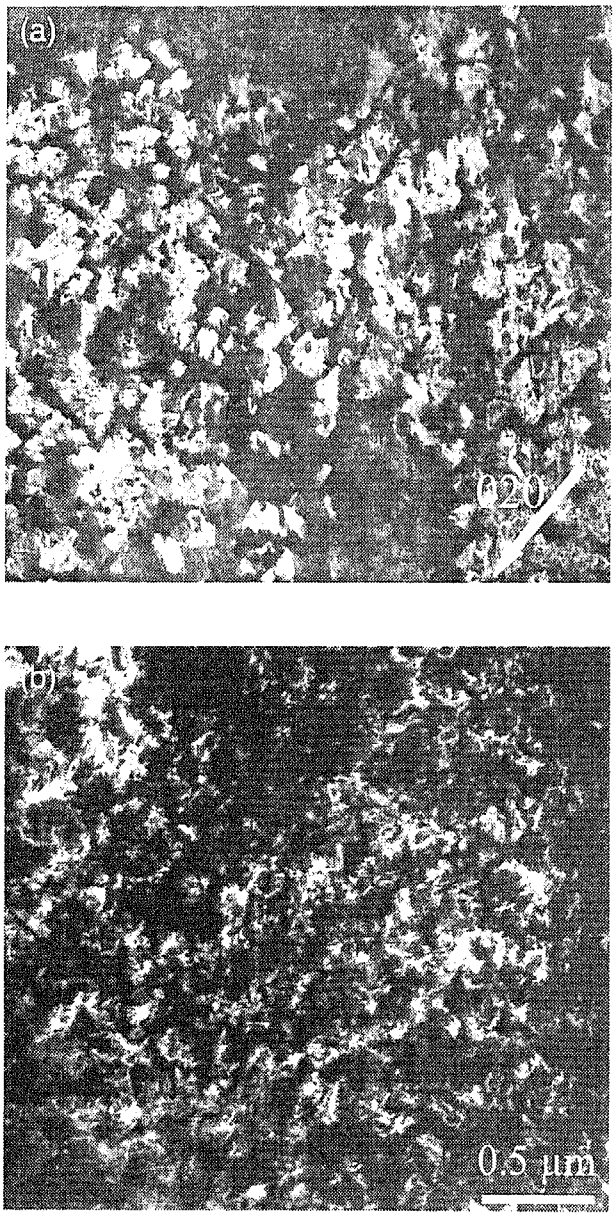

Fig. 15. Microstructure after the second poling: (a) dark-field image taken in the orientation of Fig. 14(b), using an extra spot, and (b) dark-field image using a weakly excited "normal" spot.

the compression direction is suppressed. After ferroelastic deformation, the microstructure contains regions of the size of the former colonies, with a uniform orientation of the *c*-axis.

(2) The coercive stress of ferroelastic deformation shows only a weak temperature and strain-rate dependence.

(3) The plastic flow stress of t' zirconia equals that of cubic zirconia at low temperatures. Thus, the domain and colony structure after ferroelastic deformation seems to have little influence on the flow stress.

(4) At high temperatures, the flow stress of t' zirconia is essentially higher than that of the cubic phase. This finding is explained by the athermal contributions of the long-range interaction between parallel dislocations and the back stress of bowed-out dislocation segments resulting from the interaction between dislocations of different slip systems.

(5) The main effect of the t' microstructure modified by ferroelastic deformation seems to be that it prevents recovery, which causes the decrease of the flow stress in cubic zirconia at high temperatures.

(6) Because ferroelastic deformation is also observed in partially stabilized zirconia, the present results on the motion of dislocations in a transformed colony structure can also be applied to these materials.

Acknowledgments

The authors wish to thank Christian Dietzsch and Wolfgang Greie for technical assistance.

References

[1]A. V. Virkar and R. L. K. Matsumoto, "Ferroelastic Domain Switching as a Toughening Mechanism in Tetragonal Zirconia," *J. Am. Ceram. Soc.*, **69**, C-224–C-226 (1986).

[2]A. V. Virkar, "Role of Ferroelasticity in Toughening of Zirconia Ceramics," *Key Eng. Mater.*, **153–154**, 183–210 (1998).

[3]A. H. Heuer, R. Chaim, and V. Lanteri, "The Displacive Cubic → Tetragonal Transformation in ZrO_2 Alloys," *Acta Metall.*, **35**, 661–66 (1987).

[4]C.-F. Chan, F. F. Lange, M. Rühle, J.-F. Jue, and A. V. Virkar, "Ferroelastic Domain Switching in Tetragonal Zirconia," *Mater. Res. Soc. Symp. Proc.*, **209**, 725–30 (1990).

[5]C.-F. Chan, F. F. Lange, M. Rühle, J. F. Jue, and A. V. Virkar, "Ferroelastic Domain Switching in Tetragonal Zirconia Single Crystals—Microstructural Aspects," *J. Am. Ceram. Soc.*, **74**, 807–13 (1991).

[6]R. P. Ingel, D. Lewis, B. A. Bender, and R. W. Rice, "Physical, Microstructural, and Thermomechanical Properties of ZrO_2 Single Crystals"; pp. 408–14 in Advances in Ceramics, Vol. 12, *Science and Technology of Zirconia II*. Edited by N. Claussen, M. Rühle, and A. Heuer. American Ceramic Society, Columbus, OH, 1984.

[7]K. M. Prettyman, J.-F. Jue, A. V. Virkar, C. R. Hubbard, O. B. Cavin, and M. K. Ferber, "Hysteresity Effects in 3 mol% Yttria-Doped Zirconia (t' Phase)," *J. Mater. Sci.*, **27**, 4167–74 (1992).

[8]A. V. Virkar and R. L. Masumoto, "Toughening Mechanism in Tetragonal Zirconia Polycrystalline (TZP) Ceramics"; pp. 653–63 in Advances in Ceramics, Vol. 24, *Science and Technology of Zirconia III*. Edited by S. Sōmiya, N. Yamamoto, and H. Yanagida. American Ceramic Society, Westerville, OH, 1988.

[9]J. F. Jue and A. V. Virkar, "Fabrication, Microstructural Characterization, and Mechanical Properties of Polycrystalline t'-Zirconia," *J. Am. Ceram. Soc.*, **73**, 3650–57 (1990).

[10]A. Foitzik, M. Stadtwald-Klenke, and M. Rühle, "Ferroelasticity of t'-ZrO_2," *Z. Metallkd.*, **84**, 397–404 (1995).

[11]B. Baufeld, D. Baither, U. Messerschmidt, M. Bartsch, A. H. Foitzik, and M. Rühle, "Ferroelasticity of t'-Zirconia: II, *In situ* Straining in a High-Voltage Electron Microscope," *J. Am. Ceram. Soc.*, **80**, 1699–705 (1997).

[12]B. Baufeld, D. Baither, U. Messerschmidt, and M. Bartsch, "High Voltage Electron Microscopy *In Situ* Study on the Plastic Deformation of Partially Stabilized Tetragonal Zirconia," *Phys. Status Solidi A*, **150**, 297–306 (1995).

[13]T. Kiguchi, W. Urushihara, A. Saiki, K. Shinozaki, and N. Mizutani, "Effect of Stress and Temperature on Ferroelastic Domain Switching of Partially Stabilized Zirconia Pseudo-Single Crystals," *J. Ceram. Soc. Jpn. (Int. Ed.)*, **104**, 506–11 (1996).

[14]T. Kiguchi, A. Saiki, K. Shinozaki, and N. Mizutani, "Relation between Oxygen Vacancy and Ferroelastic Domain Switching in Teragonal Zirconia Pseudo-Single Crystals," *J. Ceram. Soc. Jpn. (Int. Ed.)*, **104**, 1113–19 (1996).

[15]J. Martinez-Fernandez, M. Jimenez-Melando, A. Dominguez-Rodriguez, K. P. D. Lagerlöf, and A. H. Heuer, "High-Temperature Precipitation Hardening of Y_2O_3 Partially-Stabilized ZrO_2 (Y-PSZ) Single Crystals—II. A Quantitative Model for the Hardening," *Acta Metall. Mater.*, **41**, 3171–80 (1993).

[16]U. Messerschmidt, D. Baither, B. Baufeld, and M. Bartsch, "Plastic Deformation of Zirconia Single Crystals: A Review," *Mater. Sci. Eng. A*, **223**, 61–74 (1997).

[17]D. Baither, B. Baufeld, U. Messerschmidt, A. H. Foitzik, and M. Rühle, "Ferroelasticity of t'-Zirconia: I. High-Voltage Electron Microscopy Studies of the Microstructure in Polydomain Tetragonal Zirconia," *J. Am. Ceram. Soc.*, **80**, 1691–98 (1997).

[18]R. Gevers, J. Van Landyut, and S. Amelinckx, "The Fine Structure of Spots in Electron Diffraction Resulting from the Presence of Planar Interfaces and Dislocations (I)," *Phys. Status Solidi*, **18**, 343–61 (1966).

[19]A. H. Heuer, R. Chaim, and V. Lanteri, "Review: Phase Transformations and Microstructural Characterization of Alloys of the System Y_2O_3–ZrO_2"; see Ref. 8, pp. 3–20.

[20]B. Baufeld, D. Baither, M. Bartsch, and U. Messerschmidt, "Plastic Deformation of Cubic Zirconia Single Crystals at 1400°C," *Phys. Status Solidi A*, **166**, 127–53 (1998).

[21]U. Messerschmidt, B. Baufeld, and D. Baither, "Plastic Deformation of Cubic Zirconia Single Crystals," *Key Eng. Mater.*, **153–154**, 143–82 (1998).

[22]A. Dominguez-Rodriguez and A. H. Heuer, "Plastic Deformation of Y_2O_3 Stabilized ZrO_2 (YSZ) Single Crystals," *Cryst. Latt. Defect Amorphous Mater.*, **16**, 117–23 (1987).

[23]U. Messerschmidt, B. Baufeld, K. J. McClellan, and A. H. Heuer, "Stress Relaxation and Solid Solution Hardening of Cubic ZrO_2 Single Crystals," *Acta Metall. Mater.*, **43**, 1917–23 (1995).

[24]F. R. Chien and A. H. Heuer, "Lattice Diffusion Kinetics in Y_2O_3-Stabilized Cubic ZrO_2 Single Crystals: A Dislocation Loop Annealing Study," *Philos. Mag. A*, **73**, 2733–50 (1996).

[25]D. Baither, B. Baufeld, and U. Messerschmidt, "Defect Formation during Plastic Deformation of Y_2O_3-Partially-Stabilized ZrO_2 Single Crystals," *J. Am. Ceram. Soc.*, **78**, 1375–79 (1995). □